H and Li dynamics in $Li_{12}C_{60}$ and $Li_{12}C_{60}H_y$

N. Sarzi Amadè, M. Gaboardi, G. Magnani, M. Riccò,
D. Pontiroli, C. Milanese, A. Girella, P. Carretta and S. Sanna

Published version information

Citation: N Sarzi Amadè et al. "H and Li dynamics in $Li_{12}C_{60}$ and $Li_{12}C_{60}H_y$." International Journal of Hydrogen Energy, vol. 42, no. 35 (2017): 22544-22550. Is in proceedings of: 15th International Symposium on Metal-Hydrogen Systems, Interlaken, Switzerland, 7-12 Aug 2016.

DOI: 10.1016/j.ijhydene.2017.02.182

H and Li dynamics in $Li_{12}C_{60}$ and $Li_{12}C_{60}H_y$ ☆

N. Sarzi Amadè[a,1,*], M. Gaboardi[b,2], G. Magnani[b], M. Riccò[b], D. Pontiroli[b], C. Milanese[c], A. Girella[c], P. Carretta[a], S. Sanna.[a,3]

[a] *Department of Physics, University of Pavia, Via Bassi, 6, 27100 Pavia, Italy*
[b] *Dipartimento di Scienze Matematiche, Fisiche ed Informatiche, Università degli Studi di Parma, Via delle Scienze, 7/a, 43124 Parma, Italy*
[c] *H2-Lab, Department of Chemistry, University of Pavia, 27100 Pavia, Italy*

Abstract

Lithium and hydrogen dynamics in $Li_{12}C_{60}$ and $Li_{12}C_{60}H_y$ are investigated by means of ^{7}Li and ^{1}H solid state Nuclear Magnetic Resonance (NMR) in the temperature range 80-550 K. Differential scanning calorimeter characterization on the hydrogen sorption and desorption and X-rays structural analysis are also reported. In the pure phase, the ^{7}Li results show a thermally activated dynamic that can be associated to Li motions within the crystal interstices. Upon hydrogenation, Li ionic motion is considerably hindered by the presence of hydrofullerene molecules. The ^{1}H measurements show that C-H bonds are stable on the local scale up to 400-450 K. The NMR results at higher temperatures are compatible with a H diffusion mechanism which anticipates the H desorption process.

Keywords: Li fullerides, Solid State NMR, Hydrogen Storage

☆This document is a collaborative effort.

*Corresponding author
Email address: nicola.sarziamade@unipv.it (N. Sarzi Amadè)
[1]Dipartimento di Scienze Matematiche, Fisiche ed Informatiche, Università degli Studi di Parma, Via delle Scienze, 7/a, 43124 Parma, Italy.
[2]ISIS Facility, Rutherford Appleton Laboratory, Chilton, Didcot, Oxfordshire OX11 0QX, United Kingdom.
[3]Department of Physics and Astronomy, University of Bologna, Viale C. Berti Pichat 6/2, 40127 Bologna, Italy.

1. Introduction

Lithium cluster-intercalated fullerides (Li_xC_{60}; $x = 6 - 12$) display good performances as hydrogen absorbing materials or as potential components in ion batteries [1, 2, 3, 4, 5, 6]. In these systems, the alkali ions usually occupy the tetrahedral and octahedral interstices of the face centered cubic (*fcc*) C_{60} lattice, forming small alkali clusters [7, 8, 9, 10, 11, 12] that seem to play a fundamental role in the hydrogen absorption process, since they facilitate the H_2 dissociation. Finally, the subsequent migration of the H atoms on the negatively charged C_{60} is a reversible process. This process is characterized by significantly faster kinetics and lower hydrogenation temperature than pure C_{60} [11, 13, 14, 15, 16].

In particular, Li_6C_{60} is able to reversibly absorb up to 5 wt% H_2 [13] at moderate conditions (onset at ∼540 K), and up to 5.9 wt% H_2 is reached by addition of catalysts such as Pt/Pd nanoparticles [17]. This represents a major improvement compared to pure C_{60}, where only 2.5 wt% H_2 is chemically absorbed at rather higher temperatures and irreversibly. Moreover, Li-intercalated fullerides also demonstrated to behave as solid absorbers of indirect hydrogen carriers: for example, Li_6C_{60} can reversibly absorb up to 31.2 wt% of ammonia (corresponding to 5.5 wt% hydrogen) at mild conditions [18]. The complex hydrogenation mechanism in Li fullerides was found to originate from the catalytic activity of the Li clusters, which fill the octahedral interstices of the *fcc* C_{60} lattice. They are able to promote the H_2 dissociation, which then brings to the formation of the hydrofullerite.

$Li_{12}C_{60}$ is able to reversibly absorb up to 5 wt% H_2 with an onset temperature below 373 K [19, 15], about 150 K lower than Li_6C_{60} [13]. In both materials, after the absorption of hydrogen, a partial segregation of LiH has been identified. At low temperature (20 K), $Li_{12}C_{60}$ is a monoclinic crystal (s.g. $P2_1/c$) where the C_{60} molecules organise in a pseudo-cubic lattice with a peculiar arrangement, which allows to maximise their crowding in the [001] planes. This structure is characterized by the presence of a small cluster of five Li atoms (with a centred tetrahedron structure), residing in the pseudo-tetrahedral voids

of the parent fcc lattice, while the remaining two Li ions, which complete the stoichiometry, are delocalized in the remaining interstitial space.[20] Above 553 K the structure was determined to be fcc (s. g. $Fm\overline{3}m$), with a Li cluster in the central octahedral void and the C_{60} molecule characterized by rotational disorder [9]. Differently from the low stoichiometric compound (Li_6C_{60}), the formation of Li-H species appeared to be promoted in the first stage of hydrogenation, followed by the formation of C_{60}-H bonds [10].

Furthermore, light alkali and alkali earth (Li, Na, Mg) intercalated fullerides have been received attention also as ion conductors in the recent past, thanks to the ability of the metal ions to diffuse among the C_{60} lattice interstices already at low temperature. In particular, Li_4C_{60}, thanks to a peculiar polymeric arrangement of the fullerene units [21, 22, 23, 24], displayed a high Li-ion conductivity of 10^{-2} S/cm at room temperature (a value comparable to that observed in liquid electrolytes), with a relatively low activation energy [2]. Similarly, large Mg-ion conductivity was also observed in the Mg_2C_{60} compound, isostructural to Li_4C_{60} [25]. More recently, a detailed NMR and DC/AC conductivity study on the alkali-cluster intercalated Li_6C_{60} evidenced the presence of room temperature Li interdiffusive dinamics also in absence of fullerene polymerization, which is hampered upon the hydrogenation of the sample [5]. These findings support the possible applications of this class of compounds as solid-state electrolytes in novel ionic batteries [6, 26, 27, 4].

In this work, we report a thorough investigation of selected alkali-cluster intercalated fullerides, $Li_{12}C_{60}$ and $Li_{12}C_{60}H_y$ by means of ^{7}Li and ^{1}H solid state Nuclear Magnetic Resonance (NMR) in the temperature range 80-550 K, in order to investigate the Li and H dynamics. Differential scanning calorimeter characterization on the hydrogen sorption and desorption and x-rays structural analysis are also reported.

2. Materials and Methods

99.9% C_{60} was purchased from MER Corp. The synthesis of $Li_{12}C_{60}$ is described elsewhere [20].

$Li_{12}C_{60}$ powders were hydrogenated in a manometric instrument (PCTPro-2000, Hy-Energy&Setaram) by heating at 5 K/min from RT to 553 K at hydrogen pressure of 100 bar and appending an isothermal stage of 10 h. Desorption was performed by heating at 5 K/min the hydrogenated sample from RT to 663 K at 0.5 bar of hydrogen pressure and appending an isothermal stage of 30 min (up to plateau). The measurement was repeated twice on 2 different portions of sample to confirm the sample performance. Desorption was performed also on a small portion of hydrogenated sample by coupling the manometric instrument with a high pressure differential scanning calorimeter (Sensys DSC, Setaram) to evaluate the onset temperature and the desorption enthalpy. Desorption was performed by heating at 5 K/min from RT to 673 K at 0.5 bar of hydrogen pressure, *i.e.* the same conditions than in the manometric measurement.

X-ray powder diffraction (XRD) measurement of $Li_{12}C_{60}$ was performed on a Bruker D8 Discover powder diffractometer, working in Debye-Scherrer geometry and equipped with an area detector (GADDS) and a Cu anode. Cu-Kα_2 radiation was removed by a cross coupled double Gobel mirror. The sample was sealed in a 0.7 mm large glass capillary filled with Ar. XRD of hydrogenated sample was performed on a Bruker D5005 diffractometer (Cu-K$\alpha_{1,2}$ radiation) in the angular range 2θ=5-60° by using a suitable zero-background sample holder sealed in glove-box.

Nuclear magnetic resonance (NMR) measurements were carried out with a Tecmag Apollo spectrometer at applied magnetic field of 1.15 T in the temperature range of 80-500 K. The accuracy of the temperature is within 1 K. The ^{7}Li NMR spectra were obtained as the Fourier transform of half of the echo signal after a solid echo $\pi/2 \rightarrow \tau_{echo} \rightarrow \pi/2$ sequence of RF pulses whereas a standard Hahn echo sequence was used to obtain ^{1}H spectra. The samples (60-80 mg) were sealed in NMR grade quartz vials under 1 mbar He. A saturated

solution of LiCl(aq) (Aldrich, $\geq 99\%$) was used as reference for the shift in the ^{7}Li NMR measurements. Water was used as reference for the shift in the ^{1}H NMR measurements.

3. Results

3.1. Hydrogen absorption and desorption

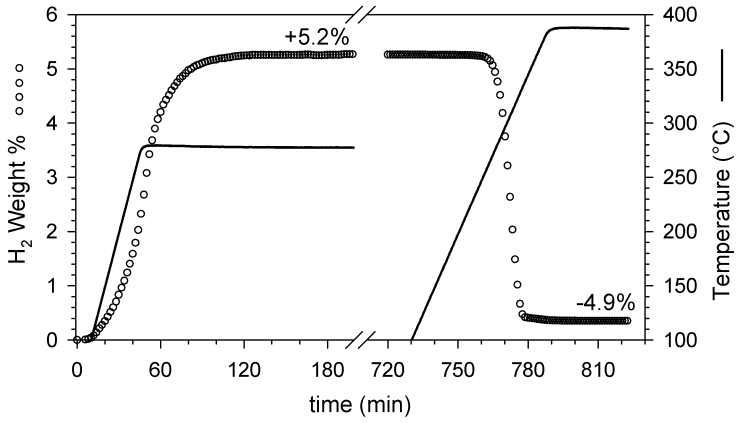

Figure 1: $Li_{12}C_{60}$ hydrogenation and dehydrogenation. The first step is performed by heating at 5°C/min from RT to 280°C at hydrogen pressure of 100 bar and appending an isothermal stage of 10 h, the second one by heating at the same rate from RT to 390 °C at 0.5 bar of hydrogen pressure followed by an isothermal stage of 30 min.

Fig.1 shows that during hydrogenation the sample starts to absorb hydrogen at 408 K and reaches a constant hydrogen content of 5.2 wt%, and in particular half of the content is absorbed during heating and half during the isothermal stage. The maximum content is reached already after 1h of isotherm treatment. Desorption starts at 548 K (value obtained by both the manometric and the calorimetric measurements) and is completed at 603 K, leading to a hydrogen release of 4.9 wt%. The reaction can be considered reversible in the limit of the experimental error of the measurement (3% of the recorded data). The measured desorption enthalpy determined by DSC for this sample is 60.5 kJ/mol H_2 (Fig.2), in agreement with previous results.[15]

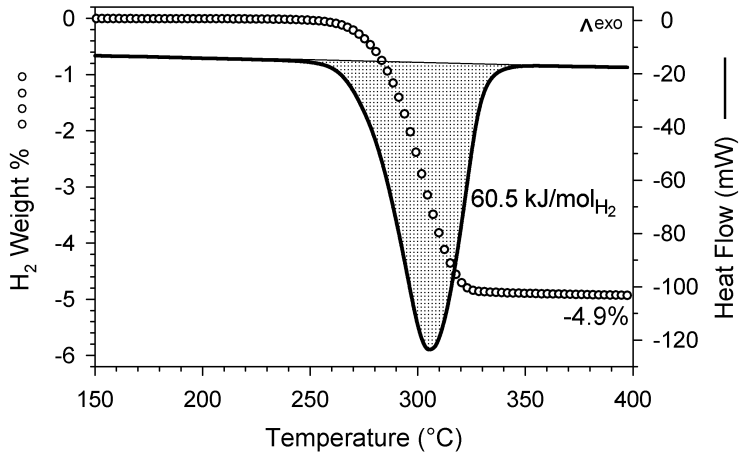

Figure 2: Coupled manometric - calorimetric measurement performed by heating the hydrogenated sample obtained as in 1 at 5°C/min from RT to 400 °C at 0.5 bar of hydrogen pressure.

3.2. X-ray Diffraction

Figure 3 displays the XRD patterns of $Li_{12}C_{60}$ and $Li_{12}C_{60}H_y$. The room temperature phase of $Li_{12}C_{60}$ is easily ascribed by the fcc cell of fullerite. Le Bail pattern decomposition of the diffractogram allowed the determination of the lattice constant, a = 13.883(7) Å (R_{wp}=11.6%). After hydrogenation, $Li_{12}C_{60}H_y$ diffractogram shows a well-defined peak at 2θ=10.35°, followed by a series of broad and convoluted peaks above 15°. The former is shifted at lower angle with respect to the 111 fcc reflection of $Li_{12}C_{60}$ and this is a typical sign of lattice expansion, easily ascribed by the larger volume occupied by a hydrofullerene compared to a C_{60} molecule. Anyway, an expanded fcc lattice does not correctly describe the positions of the other peaks; as well as the *bcc* lattice of $C_{60}H_{36}$, that is found in hydrogenated Li_6C_{60},[13] does not index the $Li_{12}C_{60}$ data. In particular, the broad shape of the other peaks and the lack of features above 22° suggest a structural disorder, possibly due to a distribution of structural units (*i.e.* a distribution of hydrofullerene molecules, with slightly different hydrogenation grade, rotation, and isomerization). The $Li_{12}C_{60}H_y$ phase was

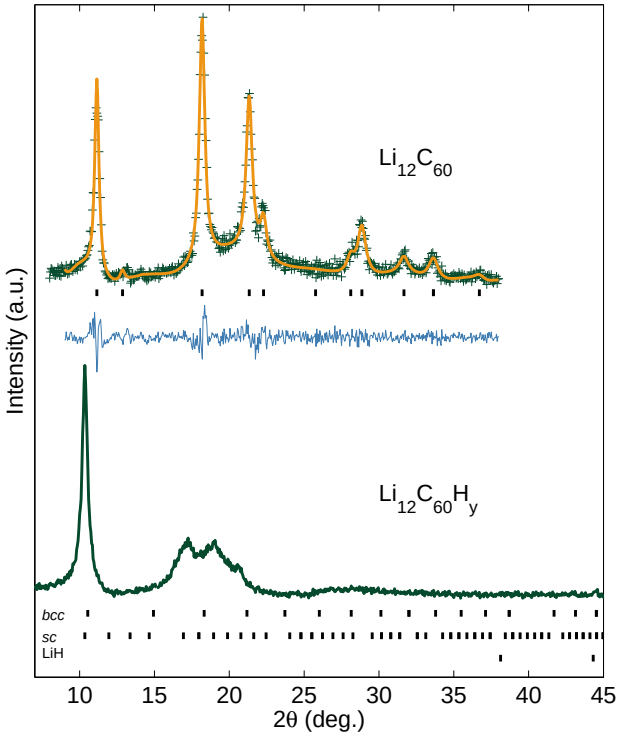

Figure 3: X-ray powder diffractions of as prepared and hydrogenated (280 °C, 100 bar H_2) $Li_{12}C_{60}$. $Li_{12}C_{60}$ diffractogram has been fit by means of Le Bail analysis (orange) with the *fcc* cell of C_{60} (R_{wp}=11.6%, $a = 13.883(7)$ Å).

tentatively indexed by a simple cubic (*sc*) cell, with an expanded cubic cell parameter of about 14.8 Å, although a lower grade of symmetry is foreseen. The presence of LiH in $Li_{12}C_{60}H_y$, although expected for this compound,[19] could not be confirmed with this type of measurement, being the lithium and hydrogen scattering factors negligible for X-rays and, thus, their diffraction below the level of detection.

3.3. ^{7}Li and ^{1}H NMR spectra

^{7}Li NMR static spectra for $Li_{12}C_{60}$ and $Li_{12}C_{60}H_y$ are displayed in Figure 4a and 4b for different temperatures. $Li_{12}C_{60}$ spectrum at 80 K can be decon-

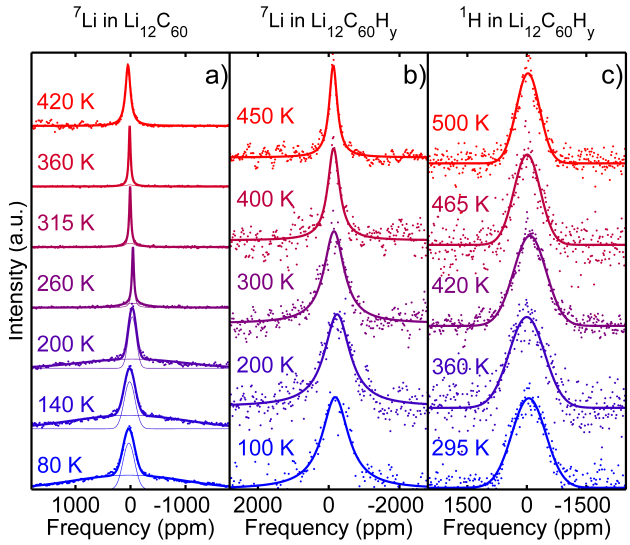

Figure 4: ^{7}Li spectra for **a)** $Li_{12}C_{60}$ and **b)** $Li_{12}C_{60}H_y$ for different temperatures. ^{1}H spectra for **c)** $Li_{12}C_{60}H_y$ for different temperatures. In panel **a)** and **b)** frequencies are in ppm with respect to ^{7}Li resonance in a saturated solution of LiCl(aq). In panel **c)** frequencies are in ppm with respect to ^{1}H resonance in water. Solid lines represent the best fit curves (see text).

voluted in two different contributions, a narrow line and a broader one, centered at the same frequency, that can be fitted by a sum of Gaussian contributions. The former can be assigned to the $1/2 \leftrightarrow -1/2$ central transition whereas the latter to the $\pm 3/2 \leftrightarrow \pm 1/2$ satellite transition, as suggested by previous results in Li_xC_{60} fullerides [5, 8]. At 80 K the corresponding full widths at half maximum (FWHM) are $\Delta\nu_{\frac{1}{2},-\frac{1}{2}} = 5.5$ kHz and $\Delta\nu_{\pm\frac{3}{2},\pm\frac{1}{2}} = 52$ kHz, respectively (Figure 5a). By increasing the temperature, a narrowing process occurs, reducing significantly both linewidths in the temperature range 180-260 K: $\Delta\nu_{\frac{1}{2},-\frac{1}{2}}$ reaches ≈ 0.8 kHz (instrumental limit/inhomogeneity of the magnetic field) whereas $\Delta\nu_{\pm\frac{3}{2},\pm\frac{1}{2}}$ reaches ≈ 7 kHz. A line narrowing is expected when the fluctuation rate of the nuclear magnetization exceeds the linewidth $2\pi\Delta\nu$ found in the static low temperature regime. This narrowing can be associated to thermally activated Li motions which trigger the spin fluctuation rate. This process may involve clusters dynamics, ion diffusion within the interstitial voids or ions hop-

ping between different interstices. Data above 360 K are not shown in Figure 5a since, in this temperature range, measurements were performed by using a furnace where the inhomogeneity of the magnetic field was ~ 2 kHz, much higher than the ^{7}Li NMR linewidth in $Li_{12}C_{60}$. On the contrary, the larger ^{7}Li and ^{1}H FWHM in $Li_{12}C_{60}H_y$ Figure 5b and c, respectively, are always negligibly affected by the instrumental linewidth also in the high temperature range.

In ^{7}Li NMR of $Li_{12}C_{60}H_y$ only a single Lorentzian line is observed over the whole investigated temperature range. In the hydrogenated phase the observation of the satellite line is prevented mainly by two factors. The first is due to the fact that during the hydrogenation, a fraction of Li atoms form lithium hydride, whose detection is prevented by its long spin-lattice relaxation time ($T_{1,LiH} \approx 8500$ s [5]), hence only the residual interstitial Li is measured yielding to a worst signal to noise ratio. In addition, the presence of hydrogen implies a significant broadening of the line, due to an additional hetero-dipolar interaction between ^{1}H and ^{7}Li magnetic moments. A gradual narrowing process is observed above $T \gtrsim 250$ K (Figure 5b). In this case another possible source of motional narrowing can be the hydrogen motion, in addition to the Li one considered above.

^{1}H NMR static spectra $Li_{12}C_{60}H_y$ are displayed in Figure 4c for different temperatures. Data can be fitted by a Gaussian line. Above 400 K the FWHM decreases from ~ 50 kHz to 35 kHz at 500 K (Figure 5b). This narrowing can be tentatively associated to the activation of H dynamics such as H diffusion on C_{60} molecule surface or H separation from fullerenes.

3.4. T_1 spin-lattice relaxations of ^{7}Li and ^{1}H

In order to further investigate the Li and H dynamics, the spin-lattice relaxation time, T_1, was measured as a function of temperature by using a standard saturation recovery pulse sequence for μ_0H= 1.15 T. A peak in the temperature evolution of the $1/T_1$ is expected when the fluctuation rate matches the Larmor frequency, *i.e.* $1/\tau_c = \omega_L$, in the present case about 120 MHz for ^{7}Li and 330 MHz for ^{1}H NMR. Since the fluctuation rate is affected by possible Li or H

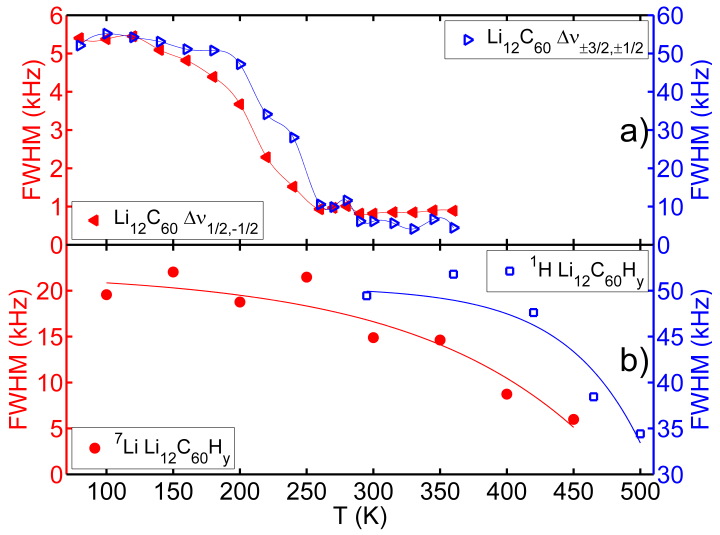

Figure 5: FWHM temperature dependance of ^{7}Li and ^{1}H spectra for **a)** $Li_{12}C_{60}$ and **b)** $Li_{12}C_{60}H_y$. The solid lines are guides to the eye.

motion, the analysis of the $1/T_1(T)$ can provide information on the correlation time and on the energy activation of the motion. The recovery of the nuclear magnetization as a function of the delay between the saturating and the readout pulses (Figure 6) can be properly fitted by the standard recovery law:

$$M(t) = M_\infty \left[1 - \exp\left(-\frac{t}{T_1}\right)^\beta\right] \tag{1}$$

where β is the stretching coefficient. In $Li_{12}C_{60}$ β is equal to 1 over the whole investigated temperature range. In $Li_{12}C_{60}H_y$ it shows a particular temperature dependance (inset in Figure 6b and 6c). In the case of ^{7}Li it slowly decreases reaching a minimum at ~ 300 K, then increasing again up to ~ 0.7. Regarding ^{1}H, β slowly increases from ~ 0.7 to 1 in the temperature range 300-400 K.

Fig.7 shows the temperature evolution of $1/T_1$ of ^{7}Li and ^{1}H for $Li_{12}C_{60}$ and $Li_{12}C_{60}H_y$. In the case of $Li_{12}C_{60}$, $1/T_1(T)$ curve shows a peak at $T \sim 400$ K; the best curve fit (solid line) is obtained by a BPP function [28]:

$$\frac{1}{T_1} \approx \frac{D\tau_c}{1+\omega_L^2\tau_c^2} + \frac{4D\tau_c}{1+4\omega_L^2\tau_c^2} \tag{2}$$

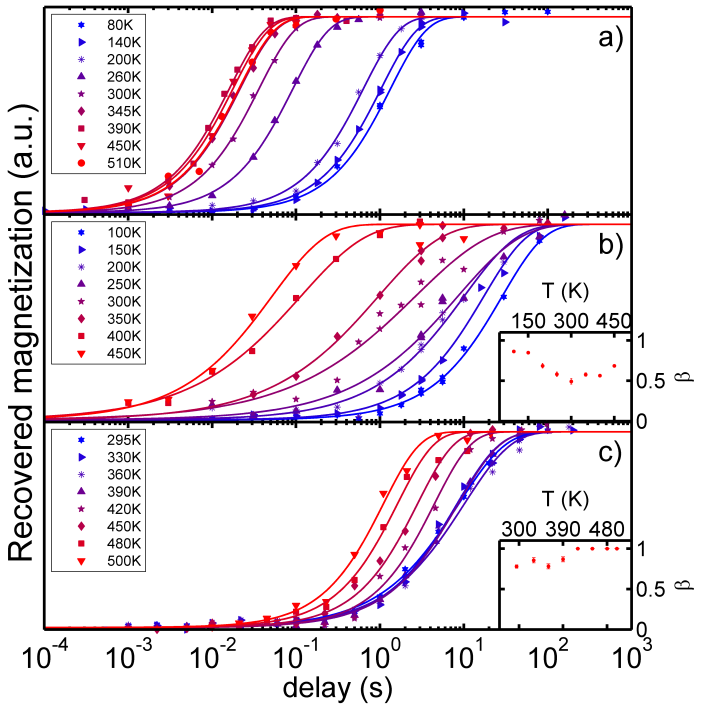

Figure 6: ^{7}Li recovered magnetization curves for **a)** $Li_{12}C_{60}$ and **b)** $Li_{12}C_{60}H_y$ at $\mu_0 H$ = 1.15 T for different temperatures. ^{1}H recovered magnetization curves for **c)** $Li_{12}C_{60}H_y$ at $\mu_0 H$ = 1.15 T for different temperatures. The solid lines are the best fit curves (see text). Inset: temperature dependance of the stretched coefficient β of Equation 1.

which considers a relaxation mechanism with a thermally activated relaxation time

$$\tau_c = \tau_\infty \exp\left(\frac{E_a}{k_B T}\right) \tag{3}$$

Here, D is a constant, E_a is the activation energy associated to the process and ω_L is the ^{7}Li Larmor frequency. In the case of ^{7}Li NMR of $Li_{12}C_{60}H_y$, the peak seems to be shifted towards higher temperature and cannot be observed completely. By considering that the BPP peak is observed when the fluctuation rate matches the larmor frequency, *i.e.* $1/\tau_c = \omega_L$, we can assume that ^{7}Li in $Li_{12}C_{60}H_y$ is in the slow motion regime for the whole range of temperature explored, *i.e.* that $\omega_L \tau_c \gg 1$. In this regime the BPP function can be

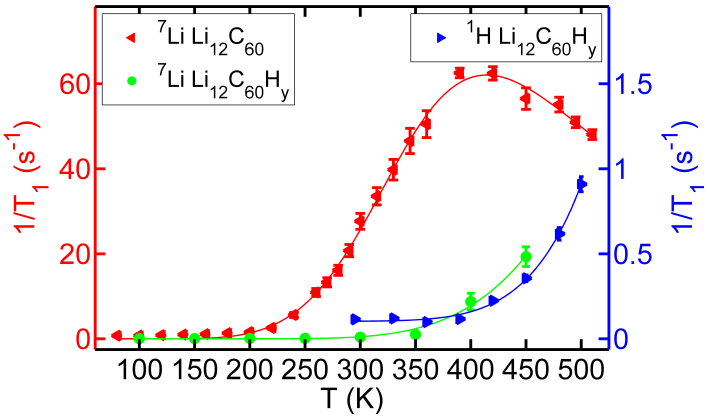

Figure 7: ^{7}Li and ^{1}H inverse spin-lattice relaxation time, $1/T_1$, vs T in $Li_{12}C_{60}$ and $Li_{12}C_{60}H_y$ at $\mu_0 H = 1.15$ T. The solid lines are the best fit curves (see text).

approximated by the following:

$$\frac{1}{T_1} \approx \frac{2D}{\omega_L^2 \tau_c} \equiv \frac{2D}{\omega_L^2 \tau_\infty} \exp\left(-\frac{E_a}{k_B T}\right) \tag{4}$$

The ^{1}H inverse spin-lattice relaxation time has been fitted to equation 4) plus a baseline. The fit outcomes for E_a are shown in Table 1.

4. Discussion

The temperature dependance of the parameter β in ^{7}Li recovery curves of $Li_{12}C_{60}H_y$ (inset in Figure 6b) indicates an higher level of disorder than the pure phase, where it is always $\beta = 1$. In fact, during the hydrogenation, a fraction of Li atoms forms LiH which segregates from the crystal [19]. This phase can be described as $Li_{12-x}C_{60}H_y$. We suppose that the residual fraction of interstitial Li is characterized by a greater disorder. β shows a minimum at T$\sim$ 300 K and then it increases up to ~ 0.7 at 450 K. We can tentatively attribute this behavior to the beginning of LiH decomposition and Li re-intercalation inside the crystal lattice. The maximum temperature investigated did not allow the observation of the end of this process which should occur when $\beta \to 1$.

The ^{7}Li $1/T_1$(T) curve in $Li_{12}C_{60}$ displayed in Figure 7 shows a single peak at $T \sim 400$ K. This behavior differs from Li_6C_{60} and Na_6C_{60} [5, 29] which shows

two peaks, one around 150 K and the other around 400 K. A recent NMR investigation [29] showed that these two peaks reflect two thermally activated ion dynamics: a local dynamics around the octahedral site (intrasite motion) and a dynamics characterised by a hopping between the tetrahedral and octahedral sites (intersite motion). Here, there is no evidence of the peak at low temperature, suggesting that the intrasite motions are hindered in $Li_{12}C_{60}$. Actually, in the low temperature phase of this system, Li clusters containing five atoms are thought to reside in the smaller pseudo-tetrahedral voids of the parent fcc lattice [20]. For steric reasons, cluster motion may be hindered in this phase. By increasing the temperature, Li-Li distance of atoms belonging to clusters increases and, consequently, at 553 K Li clusters are localised in the central octahedral void (similarly to A_6C_{60} phases - A=Li, Na) and the tetrahedral voids show a single occupancy [9]. When this structural transition occurs, ionic diffusion through the channel connecting the octahedral and tetrahedral interstices becomes possible. Therefore we associate the $1/T_1$ peak of $Li_{12}C_{60}$ in Figure 7 to the Li interdiffusion from octahedral and tetrahedral sites.

In the hydrogenated phase, the ^{7}Li NMR signal is clearly affected since both the narrowing of the linewidth in Figure 5 and the $1/T_1$ peak in Figure 7 are shifted towards higher temperatures. We suppose that the hydrogenation of fullerene definitely obstructs the channels connecting the tetrahedral and octahedral sites, hindering the ionic hopping. This is a very different behavior respect with the one observed in Li_6C_{60}, which displays the same ^{7}Li $1/T_1$(T) dependence before and after hydrogenation [5]. The high activation energy of Li reported in Tab.1 for $Li_{12}C_{60}H_y$ respect to the non hydrogenated sample might have a dual origin. On one side, the non-bcc cell of $Li_{12}C_{60}H_y$ (see Sec. 3.2) can hinder the kinetics of the intercalated Li ions, thus preventing an effective diffusion. This is hampered by the disorder induced by hydrofullerene molecules that decreases the overall symmetry, limiting the formation of diffusion channels. On the other hand, the increased amount of Li with respect to Li_6C_{60} is expected to raise the negative charge available for Li, increasing the clusterization as well as the probability to bind effectively to a hydrogen atom, forming covalent

species (as described in ref [10]).

The temperature dependence of ^{1}H NMR spectra shows a sizeable decrease of the linewidth above 400-450 K (Figure 5b). Similarly, the inverse of the relaxation rate $1/T_1$ shows a thermally activated process above 400-450 K. Two processes can be responsible for this behavior: the Li motion, not completely hindered, or the migration of H atoms on the cage of the C_{60}molecule. The latter is supported by the fact that for this material the H desorption starts around $\gtrsim$ 540 K, as shown in Sec. 3.1, hence a diffusion process in which covalently bound H would move to the neighboring C is plausible before the beginning of the desorption process. A similar diffusion process is reported for H in graphene [30]. Furthermore, we can consider that the activation energy reported for this process in Tab.1 is $E_a \sim 400$ meV, which corresponds to ~ 40 kJ/mol, the same order of magnitude of the enthalpy of the desorption process determined by DSC in Sec.3.1. Even if a direct comparison of these two energies is not possible, since the enthalpy includes also the formation of the H_2 molecule which is not regarded in the diffusion process, the fact that they have the same order of magnitude may support that they regard the H motion.

The H motion can also explain the behavior of the parameter β (inset in Figure 6c): since C-H bonds are stable on the local scale at T$\lesssim$ 400 K, the disorder can be originated by the presence of different isomers of $C_{60}H_y$ as well as a distribution of molecular hydrogenation (y in $C_{60}H_y$).; at higher temperature the fast diffusion on the surface of the fullerene makes all hydrogen atoms equivalent and $\beta \to 1$.

Table 1: Comparison of activation energies (in meV units) and correlation times (in ps units) obtained in this work from T_1 spin-lattice relaxation measurements.

Sample	Nucleus	E_a
$Li_{12}C_{60}$	^{7}Li	155(10)
$Li_{12}C_{60}H_y$	^{7}Li	~ 300
$Li_{12}C_{60}H_y$	^{1}H	~ 400

5. Conclusions

In conclusion, we investigated the hydrogen and lithium dynamics of $Li_{12}C_{60}$ on local scale in both pure and hydrogenated phases using ^1H and ^7Li NMR probes in the temperature range 80-500 K. The DSC characterization show that hydrogen absorption capability of $Li_{12}C_60$ fullerite is about 5% wt and fully reversible with a low desorption enthalpy of about 60 kJ/mol H_2.

The analysis of ^7Li NMR spectra and relaxation rate $1/T_1(T)$ in the temperature range 80-500 K revealed the presence of an ionic dynamic with an activation energy of 160 meV in the case of $Li_{12}C_{60}$ and of about 300 meV in the case of $Li_{12}C_{60}H_y$. Unlike Li_6C_{60},[5] hydrogen affects the Li dynamics in the hydrogenated phase and limits its diffusion through crystalline interstices. The ^1H linewidths of the NMR spectra and the relaxation rate $1/T_1$ confirm that the C-H bonds are stable on the local scale up to 400-450 K. Above this temperature the data are compatible with a mechanism which promotes the H diffusion on the surface of the C_{60} molecules as precursor process of the hydrogen desorption.

Acknowledgements

This work was supported by Fondazione CARIPLO [Project number 2013-0592].

References

[1] R. O. Loutfy, S. Katagiri, Fullerene Materials for Lithium-ion Battery Applications, in: Perspective of fullerene nanotechnology, 2002, pp. 357–367.

[2] M. Riccò, M. Belli, M. Mazzani, D. Pontiroli, D. Quintavalle, A. Jánossy, G. Csányi, Superionic conductivity in the Li4C60 fulleride polymer, Physical Review Letters 102 (14) (2009) 2–5. doi:10.1103/PhysRevLett.102.145901.

[3] P. Jena, Materials for hydrogen storage: Past, present, and future, J. Phys. Chem. Lett. 2 (3) (2011) 206–211. doi:10.1021/jz1015372.

[4] R. G. Zhang, F. Mizuno, C. Ling, Fullerenes: non-transition metal clusters as rechargeable magnesium battery cathodes, Chem. Commun. (Cambridge, U.K.) 51 (6) (2015) 1108–1111. doi:10.1039/c4cc08139k.
URL http://dx.doi.org/10.1039/C4CC08139K

[5] L. Maidich, D. Pontiroli, M. Gaboardi, S. Lenti, G. Magnani, G. Riva, P. Carretta, C. Milanese, A. Marini, M. Riccò, S. Sanna, Investigation of Li and H dynamics in Li6C60 and Li6C60Hy, Carbon 96 (2016) 276–284. doi:10.1016/j.carbon.2015.09.064.

[6] A. S. Cattaneo, V. Dall'asta, D. Pontiroli, M. Riccò, G. Magnani, C. Milanese, C. Tealdi, E. Quartarone, P. Mustarelli, Tailoring ionic-electronic transport in PEO-Li4C60: Towards a new class of all solid-state mixed conductors, Carbon 100 (2016) 196–200. doi:10.1016/j.carbon.2016.01.009.
URL http://dx.doi.org/10.1016/j.carbon.2016.01.009

[7] M. J. Rosseinsky, D. W. Murphy, R. M. Fleming, R. Tycko, A. P. Ramirez, T. Siegrist, G. Dabbagh, S. E. Barrett, Structural and electronic properties of sodium-intercalated C₆₀, Nature 356 (1992) 416–418. doi:10.1038/356416a0.

[8] M. Tomaselli, B. H. Meier, M. Riccò, T. Shiroka, A. Sartori, A multiple-quantum nuclear magnetic resonance study of interstitial Li clusters in LixC60, Journal of Chemical Physics 115 (1) (2001) 472–476. doi:10.1063/1.1377014.

[9] L. Cristofolini, M. Riccò, R. De Renzi, NMR and high-resolution x-ray diffraction evidence for an alkali-metal fulleride with large interstitial clusters: Li12C60, Physical Review B 59 (13) (1999) 8343–8346. doi:DOI10.1103/PhysRevB.59.8343.

[10] M. Gaboardi, C. Cavallari, G. Magnani, D. Pontiroli, S. Rols, M. Riccò, Hydrogen storage mechanism and lithium dynamics in Li12C60 investigated by μSR, Carbon 90 (2015) 130–137. doi:10.1016/j.carbon.2015.03.072.

[11] P. Mauron, A. Remhof, A. Bliersbach, A. Borgschulte, A. Züttel, D. Sheptyakov, M. Gaboardi, M. Choucair, D. Pontiroli, M. Aramini, A. Gorreri, M. Riccò, Reversible hydrogen absorption in sodium intercalated fullerenes, International Journal of Hydrogen Energy 37 (2012) 14307–14314. doi:10.1016/j.ijhydene.2012.07.045.

[12] T. Yildrim, O. Zhou, J. E. Fischer, N. Bykovetz, R. A. Strongin, M. A. Cichy, A. B. Smith III, C. L. Lin, R. Jelinek, Intercalation of sodium heteroclusters into the C60 lattice, Nature 360 (1992) 568–571. doi:10.1038/360568a0.

[13] J. A. Teprovich, M. S. Wellons, R. Lascola, S.-j. Hwang, P. A. Ward, R. N. Compton, R. Zidan, Synthesis and Characterization of a Lithium-Doped Fullerane (Lix-C60- Hy) for Reversible Hydrogen Storage, Nano Letters 12 (2012) 582–589. doi:10.1021/nl203045v.

[14] M. Aramini, M. Gaboardi, G. Vlahopoulou, D. Pontiroli, C. Cavallari, C. Milanese, M. Riccò, Muon spin relaxation reveals the hydrogen storage mechanism in light alkali metal fullerides, Carbon 67 (2014) 92–97. doi:10.1016/j.carbon.2013.09.063.

[15] P. Mauron, M. Gaboardi, D. Pontiroli, A. Remhof, M. Riccò, A. Züttel, Hydrogen desorption kinetics in metal intercalated fullerides, Journal of Physical Chemistry C 119 (4) (2015) 1714–1719. doi:10.1021/jp511102y.

[16] M. Gaboardi, S. Duyker, C. Milanese, G. Magnani, V. K. Peterson, D. Pontiroli, N. Sharma, M. Riccò, In Situ Neutron Powder Diffraction of Li6C60 for Hydrogen Storage, The Journal of Physical Chemistry C 119 (2015) 19705–19721. doi:10.1021/acs.jpcc.5b06711.

[17] M. Aramini, C. Milanese, D. Pontiroli, M. Gaboardi, A. Girella, G. Bertoni, M. Riccò, Addition of transition metals to lithium intercalated fullerides enhances hydrogen storage properties, International Journal of Hydrogen Energy 39 (2013) 2124–2131. doi:10.1016/j.ijhydene.2013.11.087.

[18] D. Pontiroli, D. D'Alessio, M. Gaboardi, G. Magnani, C. Milanese, S. G. Duyker, V. K. Peterson, N. Sharma, M. Riccò, Ammonia-storage in lithium intercalated fullerides, Journal of Materials Chemistry A (3) (2015) 21099–21105. doi:10.1039/C5TA05226B.

[19] P. Mauron, M. Gaboardi, A. Remhof, A. Bliersbach, D. Sheptyakov, M. Aramini, G. Vlahopoulou, F. Giglio, D. Pontiroli, M. Riccò, A. Züttel, Hydrogen Sorption in Li12C60, The Journal of Physical Chemistry C 117 (44) (2013) 22598–22602. doi:10.1021/jp408652t.
URL http://pubs.acs.org/doi/abs/10.1021/jp408652t

[20] F. Giglio, D. Pontiroli, M. Gaboardi, M. Aramini, C. Cavallari, M. Brunelli, P. Galinetto, C. Milanese, M. Riccò, Li12C60: A lithium clusters intercalated fulleride, Chemical Physics Letters 609 (August) (2014) 155–160. doi:10.1016/j.cplett.2014.06.036.

[21] S. Margadonna, K. Prassides, K. D. Knudsen, M. Hanfland, M. Kosaka, K. Tanigaki, High pressure polymerization of the Li-intercalated fulleride Li3CsC60, Chemistry of Materials 11 (10) (1999) 2960–2965.

[22] M. Riccò, T. Shiroka, M. Belli, D. Pontiroli, M. Pagliari, G. Ruani, D. Palles, S. Margadonna, M. Tomaselli, Unusual polymerization in the Li4C60 fulleride, Phys. Rev. B: Condens. Matter Mater. Phys. 72 (15) (2005) 1–7. doi:10.1103/PhysRevB.72.155437.

[23] D. Pontiroli, M. Riccò, T. Shiroka, M. Belli, G. Ruani, D. Palles, S. Margadonna, New polymeric phase in low-doped lithium intercalated fullerides, Fullerenes Nanotubes and Carbon Nanostructures 14 (2-3) (2006) 37–41. doi:10.1080/10407780600665967.

[24] S. Rols, D. Pontiroli, C. Cavallari, M. Gaboardi, M. Aramini, D. Richard, M. R. Johnson, J. M. Zanotti, E. Suard, M. Maccarini, M. Riccó, Structure and dynamics of the fullerene polymer Li4C60 studied with neutron scattering, Phys. Rev. B: Condens. Matter Mater. Phys. 92 (1) (2015) 014305. doi:10.1103/PhysRevB.92.014305.
URL http://link.aps.org/doi/10.1103/PhysRevB.92.014305

[25] D. Pontiroli, M. Aramini, M. Gaboardi, M. Mazzani, A. Gorreri, M. Riccò, I. Margiolaki, D. Sheptyakov, Ionic conductivity in the Mg intercalated fullerene polymer Mg2C60, Carbon 51 (2013) 143–147. doi:10.1016/j.carbon.2012.08.022.
URL http://linkinghub.elsevier.com/retrieve/pii/S0008622312006744

[26] R. Zhang, F. Mizuno, Fullerenes as high capacity cathode materials for a rechargeable magnesium battery, uS Patent App. 14/045,906 (Apr. 9 2015).
URL https://www.google.com/patents/US20150099166

[27] R. Zhang, F. Mizuno, Fullerene cathodes for a rechargeable magnesium battery, wO Patent App. PCT/US2014/055,861 (Apr. 9 2015).
URL https://encrypted.google.com/patents/WO2015050697A1?cl=de

[28] N. Bloembergen, E. Purcell, R. Pound, Relaxation effects in nuclear magnetic resonance absorption, Physical Review 73 (7) (1948) 679–715. doi:10.1103/PhysRev.73.679.
URL http://prola.aps.org/abstract/PR/v73/i7/p679{_}1

[29] N. Sarzi Amadè, D. Pontiroli, L. Maidich, M. Riccò, M. Gaboardi, G. Magnani, P. Carretta, S. Sanna, Molecular and ionic dynamics in NaxLi6-xC60, Under consideration for publication in JPCC.

[30] D. Pontiroli, M. Aramini, M. Gaboardi, M. Mazzani, S. Sanna, F. Caracciolo, P. Carretta, C. Cavallari, S. Rols, R. Tatti, L. Aversa, R. Verucchi, M. Riccò, Tracking the Hydrogen Motion in Defective Graphene,

The Journal of Physical Chemistry C 118 (13) (2014) 7110–7116. doi:10.1021/jp408339m.

URL http://pubs.acs.org/doi/abs/10.1021/jp408339m